HHS Public Access

Author manuscript

Aerosol Sci Technol. Author manuscript; available in PMC 2022 August 02.

Published in final edited form as:

Aerosol Sci Technol. 2021 July 07; 55(10): 1183–1201. doi:10.1080/02786826.2021.1938966.

Lithium-ion battery explosion aerosols: Morphology and elemental composition

Teresa L. Barone[a], **Thomas H. Dubaniewicz**[b], **Sherri A. Friend**[c], **Isaac A. Zlochower**[b], **Aleksandar D. Bugarski**[a], **Naseem S. Rayyan**[b]

[a]Health Hazards Prevention Branch, Pittsburgh Mining Research Division, National Institute for Occupational Safety and Health, Centers for Disease Control and Prevention, Pittsburgh, Pennsylvania, USA

[b]Mining Systems Safety Branch, Pittsburgh Mining Research Division, National Institute for Occupational Safety and Health, Centers for Disease Control and Prevention, Pittsburgh, Pennsylvania, USA

[c]Pathology and Physiology Research Branch, Health Effects Laboratory Division, National Institute for Occupational Safety and Health, Centers for Disease Control and Prevention, Morgantown, West Virginia, USA

Abstract

Aerosols emitted by the explosion of lithium-ion batteries were characterized to assess potential exposures. The explosions were initiated by activating thermal runaway in three commercial batteries: (1) lithium nickel manganese cobalt oxide (NMC), (2) lithiumiron phosphate (LFP), and (3) lithium titanate oxide (LTO). Post-explosion aerosols were collected on anodisc filters and analyzed by scanning electron microscopy (SEM) and energy-dispersive x-ray spectroscopy (EDS). The SEM and EDS analyses showed that aerosol morphologies and compositions were comparable to individual grains within the original battery materials for the NMC cell, which points to the fracture and ejection of the original battery components during the explosion. In contrast, the LFP cell emitted carbonaceous cenospheres, which suggests aerosol formation by the decomposition of organics within molten microspheres. LTO explosion aerosols showed characteristics of both types of emissions. The abundance of elements from the anode, cathode, and separator in respirable aerosols underscored the need for the selection of low-toxicity battery materials due to potential exposures in the event of battery thermal runaway.

CONTACT Teresa L. Barone tbarone@cdc.gov Health Hazards Prevention Branch, Pittsburgh Mining Research Division, National Institute for Occupational Safety and Health, Centers for Disease Control and Prevention, 626 Cochrans Mill Road, Pittsburgh, PA 15236, USA.

Disclaimer

The findings and conclusions in this report are those of the authors and do not necessarily represent the official position of the National Institute for Occupational Safety and Health, Centers for Disease Control and Prevention. Mention of any company or product does not constitute endorsement by NIOSH.

1. Introduction

Lithium-ion battery fires and explosions have occurred in confined spaces aboard aircraft and in airports in recent years (FAA 2020; NTSB 2014). The U.S. Federal Aviation Administration recorded 300 events from January 2006 through 2020, and while few incidents caused injuries, most led to exposures of lithium-ion battery-emitted aerosols and gases (FAA 2020). Aerosol and gas exposures in confined spaces are also a hazard for those employed by the mining industry. The mining industry supplies lithium and other metals for battery production and has become an end-user of lithium-ion batteries with the objective of replacing high-emitting diesel-powered equipment in underground operations (Paraszczak et al. 2014; Varaschin and De Souza 2015; Miller and Carriveau 2019). As the usage of lithium-ion batteries becomes more prevalent in underground mines, the chance of encountering explosions due to thermal runaway increases (Dubaniewicz and DuCarme 2013).

Thermal runaway can occur despite proper battery usage because defects in lithium-ion batteries are difficult to detect and manage (Ruiz and Pfrang 2018; Zhao, Luo, and Wang 2015). Microscopic defects in the separator that isolates the anode and cathode can cause an internal short circuit and lead to thermal runaway (Loveridge et al. 2018). Other defects such as welding flaws, electrode damage, and metal microparticle contamination can also cause an internal short circuit (Samsung 2017; Sony 2006; Loveridge et al. 2018). After a short circuit occurs, events leading to thermal runaway include exothermic reactions between battery components, an increase of pressure within the cell, and venting of aerosols and gases (Pfrang et al. 2017; Balakrishnan, Ramesh, and Kumar 2006). This is followed by rapid self-heating and the ejection of aerosols and gases (Balakrishnan, Ramesh, and Kumar 2006; Wang et al. 2012).

Emitted gases have been studied for various lithium-ion battery compositions to assess flammability and toxicity. Based on a review of experimental work published over the last two decades, major emitted gases were hydrogen, carbon monoxide, total hydrocarbons, and carbon dioxide (Baird et al. 2020). More minor but highly toxic components were hydrogen fluoride and phosphoryl fluoride (Larsson et al. 2017; Sun et al. 2016). The greater toxicity of hydrogen fluoride relative to other emitted gases was demonstrated by using fractional effective (FE) dose and FE concentration models for an LFP battery fire (Peng et al. 2020). The findings indicate that respiratory protection for acid gases would be needed in the event of lithium-ion battery thermal runaway.

In recent studies, it was shown that the composition and concentration of emitted gases depended on the battery state of charge (SOC), which is the available battery capacity expressed as a percentage of the maximum capacity (Yang et al. 2021; Chen et al. 2020a, 2020b; Mao et al. 2019). For example, batteries with greater SOC emitted higher concentrations of carbon monoxide and benzene due to differences in internal reactions (Yang et al. 2021; Chen et al. 2020a). The nature of internal reactions was investigated for battery materials in states of overcharge (100–150% SOC) by using scanning electron microscopy (SEM) and differential scanning calorimetry (DSC) (Mao et al. 2019). The SEM analysis indicated that lithium deposited on the anode and reacted with the electrolyte

to generate heat and initiate thermal runaway. In addition, the SEM and DSC analyses suggested that cathode delithiation led to violent reactions between the cathode and electrolyte and contributed to thermal runaway (Mao et al. 2019).

Aerosols emitted by lithium-ion battery thermal runaway have not been characterized to the authors' knowledge. In particular, information is lacking on the size, composition and morphology of explosion aerosols in the respirable size range (e.g., ≤4 μm). However, the powder deposited after lithium-ion battery thermal runaway has been studied for 8.5–300 μm particles (Chen, Wang, and Yan 2020). The study was carried out for a single battery type with an NMC cathode and showed that powder samples contained carbon, organic compounds, carbonates, and transition metals. The transition metal content of mixed aerosols can especially influence toxicity. In mixtures with carbonaceous particles, transition metals mediate the production of reactive oxygen species that cause oxidative damage, such as DNA strand breaks and inflammation (Donaldson et al. 1997; Valavanidis, Salika, and Theodoropoulou 2000; Jiménez et al. 2000; Wilson et al. 2002; Knaapen et al. 2002). Whether transition metals and other powder components are present in aerosols in the respirable size range has not been reported previously to the authors' knowledge. The absence of such information presents a challenge when adequately identifying hazards and specifying requirements of control strategies for respiratory protection.

In the current study, lithium-ion battery explosion aerosols were characterized for three commercially available battery types. The original battery components and emitted aerosols were analyzed by SEM and energy-dispersive x-ray spectroscopy (EDS) to determine the morphology and elemental composition of the anode, cathode and separator materials and corresponding explosion aerosols. Aerosol samples were filter collected and analyzed off-line, which prevented the corrosion of on-line aerosol instrumentation by hydrogen fluoride in the explosion gas and enabled the objective of characterizing potential aerosol exposures. The current study provides the first systematic characterization of lithium-ion battery explosion aerosols and is an important part of health and safety assessments.

2. Methods

Each lithium ion battery cell was subjected to high temperatures in an accelerating rate calorimeter (ARC) to initiate thermal runaway. After battery thermal runaway and cell explosion, emitted aerosols were collected by filtration at the outlet of the ARC. The collected aerosols were analyzed by SEM and EDS, and the elemental compositions were compared with the original battery materials.

2.1. Thermal runaway initiation

The battery cells were cylindrical spiral-wound types 18650 (NMC and LTO) and 26650 (LFP) with rated capacities of 3.2, 3.8, and 1.3 Ah for NMC, LFP and LTO batteries, respectively. The cells were conditioned with three charge-discharge cycles followed by a charge to 100% SOC. A multi-channel potentiostat/galvanostat (Arbin Instruments, College station, TX, Model MSTAT) was used to cycle the cells following cell-manufacturer-specified parameters. Observed discharge capacities were at least 97% of rated capacity. The

activation process occurred during the ARC test, and the battery short circuited internally before thermal runaway.

Thermal runaway was initiated using an EV + ARC system (Thermal Hazard Technology (THT), Milton Keynes, UK). The EV + ARC instrumentation included type N thermocouples. One of the thermocouples was taped to the metallic surface of the battery cell, about mid-length, with fiber tape, and the other was inserted into free space near the sampler inlet. Sensor data were recorded by the THT ARC enhanced system (ARCes) control and data acquisition software.

The battery cell was mounted in the EV + ARC and the samplers were positioned just outside the port of the EV + ARC (Figure 1). The ARC temperature was raised at a constant rate to provide steady-state heating until the cell reached thermal runaway (Figure 2). The heaters were shut off after thermal runaway detection. The battery cell explosion and emitted plume were viewed using a video camera mounted at the window of the explosion vessel.

2.2. Explosion aerosol sampling

As the emitted plume filled the EV + ARC and passed through the outlet, aerosol samples were collected by filtration for 5 s at 1 liter per minute. The sampling rates were minimized to avoid oversampling for microscopy analysis. Aerosols were collected on 25-mm anodisc filters with 200 nm pore size (Whatman, Cytiva, Marlborough, MA, USA) using stainless-steel filter holders and sample probes with a 0.64-cm diameter and 7- to 23-cm length. Probes of different lengths were used to vary the distance of the filter holder from the hot plume. However, this precaution was unnecessary since the temperature at the sample inlet did not exceed 50 °C during each sampling despite the inlet being only 9 cm from the EV + ARC port (Figures 1 and 2) and 42 cm from the battery position. Background aerosols were collected in the ARC blast enclosure and were found to be negligible (~2 particles per sample).

2.3. SEM and EDS analysis

The morphology and elemental composition of explosion aerosols and battery materials (anode, cathode, and separator) were analyzed by SEM (Model S-4800, Hitachi, Tokyo, Japan) and EDS (Bruker Quantax, Madison, WI, USA), respectively. Samples were extracted from the batteries after fully discharging the cells for personnel safety. The batteries were discharged before disassembling for materials characterization because equipment was not available to disassemble the battery at 100% SOC, such as an argon-filled glove box containing water below 0.1 ppm and oxygen below 2.0 ppm, which was used by Mao et al. (2019). Although the battery materials were not evaluated at 100% SOC, the results on the elements present in the anode, cathode and separator were consistent with the expected elemental compositions for commercial lithium ion batteries and helped to understand their presence in the emitted aerosols. One of the main differences that can be expected between batteries at 0% and 100% SOC is the difference in the distribution of lithium (Mao et al. 2019). However, lithium could not be measured using the current method because the SEM was not equipped with a windowless EDS detector that measures very light elements.

The aerosol filters and anode, cathode and separator films were mounted on 25-mm aluminum posts using conductive carbon tape. The low conductivity samples (explosion aerosols and separator film) were sputter coated with a conductive layer of gold and palladium to avoid image distortion from charge accumulation. Because the aerosol filters had especially low conductivity, the samples had to be sputter coated for 4 min, while the separator film only required a 2-min coating to improve image clarity. The additional conductive coating did not interfere with the analysis of aerosol morphology and composition. Images were acquired at 5 and 20 kV and 10^3–5×10^4 magnification, and elemental compositions were analyzed at 20 kV. Elemental maps of individual and agglomerated particles were acquired as element distribution images using ESPRIT software (version 2.2, Bruker, Madison, WI, USA) with 90 s capture time (mapping scan time).

3. Results and discussion

3.1. Battery materials characterization

Lithium-ion batteries were characterized to obtain information on the source materials that contributed to aerosol formation in the study. The characterized materials were the anode, cathode, and separator of the spiral-wound battery cells. These components can vary between manufacturers and may contain toxic materials. Other components, such as the charge collectors and cell casing, have common compositions of copper, aluminum and steel (Liao et al. 2019; Wierzbicki and Sahraei 2013) and were not a focus of the current study.

An additional component that can contribute to aerosol formation is the electrolyte solution, which is often a lithium salt dissolved in an organic carbonate solvent (Harris, Timmons, and Pitz 2009; Balakrishnan, Ramesh, and Kumar 2006). An organic carbonate solvent was identified previously in a battery selected for the current study by using Fourier transform infrared spectroscopy (FTIR) (Dubaniewicz et al. 2021). While FTIR provides molecular composition, EDS can only provide elemental composition for nonvolatile materials in the high vacuum environment of the SEM. Consequently, solvent composition could not be evaluated by the currently used method. However, the anode, cathode, and especially the separator can retain elements of the lithium salt component of the electrolyte solution. Those elements appeared in EDS spectra and are reported in the results.

3.1.1. Anodes—In lithium-ion batteries, the electrodes are often composed of an active material, a conductive filler, and a polymer binder (Massé et al. 2017). Several active materials are being developed for anodes. Two that have been widely commercialized are graphite and titanate (Massé et al. 2017; Nitta et al. 2015). The SEM and EDS analyses suggest that these common active materials were used in the batteries selected for the current study. The EDS spectra show a strong carbon peak (Figures 3a and b), and the SEM images display super-micron faceted particles (Figures 4a and b), which suggests that the active material was graphite for the NMC and LFP anodes. The graphite particles of the NMC anode were larger and more uniform than the LFP anode (Figures 4a and b). The relatively large particle size and uniform morphology can enhance battery tolerance of thermal abuse (Park and Lee 2009; Adams et al. 2019). The NMC anode may have been manufactured with better thermal abuse tolerance in order to compensate for the relatively reactive cathode

materials. The weak peaks for fluorine and phosphorous (Figures 3a and b) suggest that the NMC and LFP anodes contained a small amount of lithium salt from the electrolyte solution (e.g., lithium hexafluorophosphate) (Harris, Timmons, and Pitz 2009; Campion et al. 2004). The carbon and fluorine content of the anode appeared in explosion aerosols as will be shown in Section 3.2.

The SEM and EDS results for the third battery type indicated that the anode consisted of lithium titanate. The anode material had strong titanium and oxygen peaks (Figure 3c) and consisted of submicron faceted particles (Figure 4c). The morphology is consistent with a lithium titanate anode shown by Masoud and Indris (2015). In addition, the carbon peak in EDS spectra, and the interspersed nanoparticle aggregates and surface coating in SEM images indicated a conductive carbon filler and polymer binder (Massé et al. 2017). The active material, filler and binder may have contributed to the explosion aerosol emissions discussed in Section 3.2.

3.1.2. Cathodes—Transition metals are commonly used as cathode materials because of their high energy storage capability and the traditionally held view of their significant role in lithium intercalation (ions function as the electron acceptor upon insertion of lithium) (Nitta et al. 2015; Ceder et al. 1998). A widely commercialized composite of transition metals was present in a battery selected for the current study (NMC) as shown by the representative EDS spectrum of nickel, manganese, and cobalt in Figure 5a. The ratio of nickel to manganese and cobalt approached 8:1:1, which is a composition known for its high specific capacity. However, this composition also has a shorter life cycle and lower thermal abuse tolerance than another common ratio of 5:2:3 (Nitta et al. 2015). Consequently, this battery type is relevant for the current evaluation because of its potential for thermal runaway and because the materials are a potential source of toxic components in explosion aerosols.

The cathode of the second battery type contained phosphorous and iron (Figure 5b) in micron to submicron spheroidal particles (Figure 6b). These characteristics suggest that the cathode contained the common active material, lithium iron phosphate. The iron content is a health concern because its inhalation can lead to the generation of reactive oxygen species that cause DNA damage (Donaldson et al. 1997). However, iron is less toxic than other transition metals, such as those in the NMC cathode. For example, exposure to 5 mg iron/m^3 leads to minor adverse health effects (NIOSH 1994), while exposure to a thousand times lower concentration of cobalt (0.005 mg/m^3) can lead to asthma, pneumonia, and wheezing (ATSDR 2004). Cobalt was also a major component of the cathode of the third battery type (LTO) and was present along with manganese as shown by the representative spectrum in Figure 5c. Both species are of concern as inhalation of high levels of manganese can lead to disabling neurological effects (ATSDR 2012).

The comparison of particle morphology for the three cathodes showed that the NMC active material was more tightly fused in large clusters (Figure 6a) than the LTO cell, which had more loosely agglomerated active material held together by binder material (Figure 6c). The NMC and LTO cathodes consisted of larger particles than the LFP cathode (Figure 6b). The

smaller particles of the LFP cathode are more likely to be heated throughout and vaporized in a flash event like an explosion.

3.1.3. Separators—Separators play an important role in battery safety by isolating the anode from the cathode to prevent a short circuit and thermal runaway. A common separator with low production cost is the porous polymer membrane. Porous polymer membranes have good lithium-ion conductivity, but the organic membrane can fail at high temperatures and can be vulnerable to punctures by lithium dendrites (Nestler et al. 2014; Duan et al. 2020). More resistant separators composed of ceramic and organic composites have become common in commercial batteries in the last decade (Nestler et al. 2014). The current results suggest that ceramic composites were used in two of the three batteries selected for the study. In the NMC and LFP batteries, there were strong peaks for aluminum and oxygen along with a slight peak for carbon in the separator spectra (Figures 7a and b). This composition and the agglomerate morphology (Figures 8a and b) suggest that porous ceramic membranes of alumina or lithium aluminate were used along with an organic coating or membrane (Nestler et al. 2014; Raja et al. 2015). In contrast, the LTO separator contained mostly carbon (Figure 7c) and the morphology was consistent with porous polymer membranes (Figure 8c) (Nestler et al. 2014). Therefore, carbon in explosion aerosols could be attributed to LTO separator materials and the small amount of carbon in other areas (the LTO anode and cathode). The presence of aluminum in explosion aerosols could be attributed to the separator materials and the charge collector.

3.2. Explosion aerosols analysis

3.2.1. Thermal runaway—Thermal runaway was initiated at 145, 200, 163 °C for the NMC, LFP, and LTO cells, respectively (Yuan et al. 2020). As thermal runaway progressed, the batteries exploded in different manners. The NMC cell exploded more intensely and over a shorter period than the LFP and LTO cells (Figure 9; Dubaniewicz et al. 2021). The explosion caused the NMC cell to be ejected from the sample holder and to emit abundant embers that streaked across the chamber (Figure 10a). In contrast, the LFP and LTO cells remained in the sample holder and continuously emitted smoke (Figures 10b and c). Less smoke appeared in the video of the LTO explosion than the LFP explosion (Figures 10b and c). Another difference was that the LTO cell contents were partially ejected from the cell housing (Figure S1). The differences in explosions probably influenced the aerosol emissions. It was estimated that more aerosols were emitted by the NMC cell than the LFP and LTO cells based on the greater amount of sample collected in a 5-sec sampling period.

3.2.2. NMC cell—Although the sampling period for the NMC cell was only a few seconds, a large amount of aerosols were collected (Figure 11), and EDS mapping was needed to distinguish between particles that overlapped on the sample substrate. Using the mapping technique, it was found that the explosion aerosols were of three main types: (1) fragments of the anode or cathode, (2) microspheres, and (3) nanoparticles. The anode-type fragments in explosion aerosols were faceted carbonaceous particles (Figure 12) similar to the battery material in Figure 4a. The cathode-type fragments contained nickel, manganese, and cobalt (Figure 13) and had a morphology comparable to the battery material in Figure 6a. The anode and cathode fragments had sizes in the range of 5–10 μm, which is the upper

size range included in the international convention for respirable aerosols. The international convention for respirable aerosols defines efficiencies at which particles of a given size range are sampled to assess relevant exposures (e.g., Approximately 30% at 5 μm, 1% at 10 μm) (CEN 1993; ISO 1995; ACGIH 2014). Respirable aerosols are a health concern because they can penetrate to unciliated regions of the respiratory tract and influence adverse health effects.

Exposure limits (in terms of threshold limit values) recommended by the American Conference of Government Industrial Hygienists (ACGIH) are 1.5 mg/m^3 for nickel, 0.02 mg/m^3 for cobalt, and 0.02 mg/m^3 for manganese (ACGIH 2018), which suggests more stringent guidelines for explosion aerosols containing cobalt and manganese. Adverse health effects associated with cobalt inhalation include asthma, pneumonia, and wheezing, and manganese exposure can lead to disabling neurological effects (ATSDR 2004, 2012). Recommended exposure limits for metals given by the ACGIH are based on the concentration of the metal element rather than the molecular composition, such as the oxide or salt. In addition, metal elements have been given toxicological profiles by the U. S. Agency for Toxic Substances and Disease Registry (ATSDR), in which the adverse health effects of various molecular compositions are discussed. The toxicological profile for cobalt suggests that the inhalation of the pure metal, oxide, and salt leads to significant adverse health effects (ATSDR 2004). A comparison of the molecular compositions for each element is beyond the scope of the current study, but the toxicological profiles with pertinent information are referenced.

The microspheres in NMC explosion aerosols varied in elemental composition. The most common compositions were nickel (Figure 14a), aluminum (Figure 14b), and a mixture of carbon, fluorine, and oxygen (Figure 14c). Nickel particles were clearly distinguishable from the background substrate because nickel had a strong EDS signal that differed from the substrate material (Figure 14a). However, the aluminum microspheres matched the aluminum substrate, so their shape was not discerned in the EDS map (Figure 14b). Still, aluminum could be identified because when other elements were present, the aluminum signal weakened, and other elements became more apparent. For example, carbon, fluorine, and oxygen generally have weak EDS signals, but they were more apparent than the aluminum in the center of Figure 14c. The mixture of carbon, fluorine, and oxygen suggests the source may have been the electrolyte solution, which is often composed of a lithium hexafluorophosphate salt and an organic carbonate solute (Harris, Timmons, and Pitz 2009; Balakrishnan, Ramesh, and Kumar 2006). The sources of aluminum were the separator membrane and the cathode charge collector (Section 3.1.3), and nickel microspheres originated from the cathode material (Section 3.1.2).

These compositions have been associated with adverse health effects. The inhalation of nickel aerosols is associated with lung inflammation and lung cancer (ATSDR 2005), and inhalation of aluminum can cause a persistent cough and adversely affect the nervous system (ATSDR 2008). The health effects of aerosols containing carbon, fluorine, and oxygen will strongly depend on molecular composition, which could not be determined by EDS. Overall, their composition can especially impact respiratory health because the microspheres were in a size range that efficiently penetrates to the lung (0.1 to 3 μm). The penetration efficiencies

approximated by the international convention for respirable aerosols are 99.7% for 0.1 μm and 74% for 3 μm (CEN 1993; ISO 1995; ACGIH 2014).

The nanoparticles in NMC explosion aerosols had diameters from 30 to 100 nm. Particles in this size range are a health concern because of their substantial penetration to the lung and biologically active surface area. Most were present as aggregates because of particle overlap on the sample substrate and their tendency to coagulate in the aerosol phase (Figure 15). Their low effective density made it difficult to determine composition by EDS. They may have been composed of carbon, which has a weak EDS signal. However, in an area with a thick layer of aggregates (near a large carbon particle), they appeared to be composed of aluminum (Figure 16). This will be evaluated in a future study using a different substrate. Considering possible sources, the aluminum in the separator (ceramic) and the carbon in the anode (graphite) are not easily vaporized and re-condensed to form nanoparticles. In addition, only a small amount of carbon was used as conductive filler and polymer binder in the separator and cathode (Figures 5 and 7). Therefore, given the abundance of nanoparticles and the expectation of a large source, it is more likely that the nanoparticle source was the aluminum charge collector near the cathode (Figure S2). Thermal runaway may have heated the aluminum charge collector causing it to vaporize and re-condense to form nanoparticles.

3.2.3. LFP cell—LFP explosion aerosols were more homogenous in morphology and elemental composition than the aerosols emitted by the NMC cell explosion. They appeared to consist mostly of cenospheres (hollow spheres) in the respirable size range (0.6–5 μm) (Figures 17 and 18) and contained carbon, silicon, and fluorine (Figure 19). The major source of these aerosols may be the anode due to its carbon and fluorine content (Figure 3b), and also because silicon is a common anode constituent that is used to increase capacity. In general, silicon swells from the charging process, and this swelling can reduce the life of the battery cell. However, small amounts of silicon may be added to graphite anodes to increase capacity without substantially affecting the life of the cell (Yim, Courtel, and Abu-Lebdeh 2013). A small amount of silicon may go undetected by EDS but can become enriched during the explosion. For example, the enrichment of silicates occurs during the combustion of pulverized coal and leads to the formation of cenospheres in fly ash (Ranjbar and Kuenzel 2017). By a similar process, the graphite anode may have served as the source of cenospheres in LFP explosion aerosols. Material with an irregular morphology was found to contain carbon only (Figure 20). The irregular material may have been cenospheres that collapsed due to the lack of a silicon-containing shell to withstand the internal gas pressure from organic decomposition. Transition metals (e.g., iron) were absent from LFP aerosols, and this contrasts sharply with the results for NMC explosion aerosols.

3.2.4. LTO cell—Aerosols emitted by the LTO explosion had similar characteristics to the emissions of the LFP and NMC cells. Like LFP aerosols, the typical morphologies were spheroids and cenospheres in the respirable size range (0.1–4 μm) (Figure 21). Some cenospheres had a porous structure as shown in Figure 22. Porous cenospheres are thought to form by the release of trapped gases through channels in high viscosity molten droplets (Ranjbar and Kuenzel 2017). Probably due to their substantial void space and low effective density, an EDS signal was not apparent.

Similar to the NMC emissions, elements from the anode and cathode were present in respirable aerosols. Those containing cobalt from the cathode and titanium from the anode were less common than cenospheres. However, they were more easily characterized due to their strong EDS signals (Figure 22 and Figure S3, supplementary material). It was observed that fewer aerosols were emitted relative to the NMC cell by comparing Figures 11 and 21. Despite their lower abundance, LTO explosion aerosols may still be hazardous because the inhalation of even a small amount (5 $\mu g/m^3$) of cobalt is associated with adverse health effects including wheezing and pneumonia (ATSDR 2004).

The concentration of emitted aerosols was not quantified because a specially designed experimental setup would be needed, and its construction and implementation were beyond the scope of the current study. The experimental setup should be constructed so that the explosion aerosols are well mixed before sampling, or the total aerosol from the explosion should be collected to enable quantification. Sampling a well-mixed aerosol is important because the spatial variation of aerosols is much more pronounced than for gases due to weaker diffusion. The aerosol mixing system or total aerosol sampling system should be integrated with the ARC, which was not originally designed for this purpose. The quantification of concentration will be considered for a future study.

4. Conclusions

To better understand potential exposures, the characteristics of aerosols emitted by lithium-ion battery explosions were studied by SEM and EDS. The SEM and EDS analyses showed that the NMC, LFP, and LTO battery explosions emitted abundant aerosols in the respirable size range. NMC aerosols consisted of 0.03–0.1 μm nanoparticles, 0.1–3 μm microspheres, and 5–10 μm anode and cathode fragments. The NMC aerosols were more numerous and contained a wider size range than the other battery aerosol emissions. The cathode fragments contained the transition metals, nickel, manganese, and cobalt; and the microspheres were composed of nickel, aluminum, or a mixture of carbon, fluorine, and oxygen. There appeared to be a greater transition metal content in NMC aerosols than the other battery emissions. LFP aerosols were more homogenous in morphology and composition and largely consisted of cenospheres (0.6–5 μm) that contained carbon, silicon, and fluorine. Cenospheres (0.1–4 μm) were also observed in LTO explosion emissions, as were particles containing cobalt and titanium. Since cobalt and other transition metals, were present in NMC/LTO but not LFP samples, LFP explosion aerosols may be the least hazardous of the three battery types evaluated.

Supplementary Material

Refer to Web version on PubMed Central for supplementary material.

Acknowledgments

The authors thank Jon Hummer and John Soles of NIOSH for assistance with the experimental setup.

References

ACGIH, American Conference of Governmental Industrial Hygienists. 2014. TLVs and BEIs: Based on the documentation of the threshold limit values for chemical substances and physical agents & biological exposure indices. ACGIH Publication No. 0114, Cincinnati, OH.

ACGIH, American Conference of Governmental Industrial Hygienists. 2018. TLVs and BEIs: Based on the documentation of the threshold limit values for chemical substances and physical agents & biological exposure indices. ACGIH Publication No. 0118, Cincinnati, OH.

Adams RA, Mistry ANAN Mukherjee P. P. Pol, and V G. 2019. Materials by design: Tailored morphology and structures of carbon anodes for enhanced battery safety. ACS Applied Materials & Interfaces 11 (14): 13334–42. doi: 10.1021/acsami.9b02921. [PubMed: 30892862]

ATSDR, Agency for Toxic Substances and Disease Registry. 2004. Toxicological profile for cobalt. U.S. Department of Health and Human Services, Public Health Service, Atlanta, GA.

ATSDR, Agency for Toxic Substances and Disease Registry. 2005. Toxicological profile for nickel. U.S. Department of Health and Human Services, Public Health Service, Atlanta, GA.

ATSDR, Agency for Toxic Substances and Disease Registry. 2008. Toxicological profile for aluminum. U.S. Department of Health and Human Services, Public Health Service, Atlanta, GA.

ATSDR, Agency for Toxic Substances and Disease Registry. 2012. Toxicological profile for manganese. U.S. Department of Health and Human Services, Public Health Service, Atlanta, GA.

Baird AR, Archibald EJ, Marr KC, and Ezekoye OA 2020. Explosion hazards from lithium-ion battery vent gas. Journal of Power Sources 446:227257. doi: 10.1016/j.jpowsour.2019.227257.

Balakrishnan PG, Ramesh R, and Kumar TP 2006. Safety mechanisms in lithium-ion batteries. Journal of Power Sources 155 (2):401–14. doi: 10.1016/j.jpowsour.2005.12.002.

Campion CL, Li W, Euler WB, Lucht BL, Ravdel B, DiCarlo JF, Gitzendanner R, and Abraham KM 2004. Suppression of toxic compounds produced in the decomposition of lithium-ion battery electrolytes. Electrochemical and Solid-State Letters 7 (7):A194. doi: 10.1149/1.1738551.

Ceder G, Chiang YM, Sadoway DR, Aydinol MK, Jang YI, and Huang B. 1998. Identification of cathode materials for lithium batteries guided by first-principles calculations. Nature 392 (6677):694–6. doi: 10.1038/33647.

CEN, European Committee for Standardization. 1993. Workplace atmospheres – Size fraction definitions for measurement of airborne particles. CEN Standard EN 481, CEN-CENELEC Management Centre, Brussels, Belgium.

Chen S, Wang Z, and Yan W. 2020. Identification and characteristic analysis of powder ejected from a lithium ion battery during thermal runaway at elevated temperatures. Journal of Hazardous Materials 400:123169. doi: 10.1016/j.jhazmat.2020.123169.

Chen S, Wang Z, Wang J, Tong X, and Yan W. 2020a. Lower explosion limit of the vented gases from Li-ion batteries thermal runaway in high temperature condition. Journal of Loss Prevention in the Process Industries 63: 103992. doi: 10.1016/j.jlp.2019.103992.

Chen S, Wang Z, Yan W, and Liu J. 2020b. Investigation of impact pressure during thermal runaway of lithium ion battery in a semi-closed space. Applied Thermal Engineering 175:115429. doi: 10.1016/j.applthermaleng.2020.115429.

Donaldson K, Brown DM, Mitchell C, Dineva M, Beswick PH, Gilmour P, and MacNee W. 1997. Free radical activity of PM10: Iron-mediated generation of hydroxyl radicals. Environmental Health Perspectives 105 (Suppl 5): 1285–9. doi: 10.1289/ehp.97105s51285. [PubMed: 9400739]

Duan J, Tang X, Dai H, Yang Y, Wu W, Wei X, and Huang Y. 2020. Building safe lithium-ion batteries for electric vehicles: A review. Electrochemical Energy Reviews 3 (1):1–42. doi: 10.1007/s41918-019-00060-4.

Dubaniewicz TH, and DuCarme JP 2013. Are lithium ion cells intrinsically safe? IEEE Transactions on Industry Applications 49 (6):2451–60. doi: 10.1109/TIA.2013.2263274. [PubMed: 26166911]

Dubaniewicz TH, Zlochower I, Barone T, Thomas R, and Yuan L. 2021. Thermal runaway pressures of iron phosphate lithium-ion cells as a function of free space within sealed enclosures. Mining, Metallurgy & Exploration 38 (1):539–47. doi: 10.1007/s42461-020-00349-9.

FAA, Office of Security and Hazardous Materials Safety. 2020. Events with smoke, fire, extreme heat or explosion involving lithium batteries. Battery Incident Chart. Accessed December 16, 2020. https://www.faa.gov/hazmat/resources/lithium_batteries/media/Battery_incident_chart.pdf.

Harris SJ, Timmons A, and Pitz WJ 2009. A combustion chemistry analysis of carbonate solvents used in Li-ion batteries. Journal of Power Sources 193 (2):855–8. doi: 10.1016/j.jpowsour.2009.04.030.

ISO, International Organization for Standardization. 1995. Air quality—particle size fraction definitions for health-related sampling. ISO 7708:1995. International Organization for Standardization, Geneva, Switzerland.

Jiménez LA, Thompson J, Brown DA, Rahman I, Antonicelli F, Duffin R, Drost EM, Hay RT, Donaldson K, and MacNee W. 2000. Activation of NF-κB by PM10 occurs via an iron-mediated mechanism in the absence of IκB degradation. Toxicology and Applied Pharmacology 166 (2):101–10. doi: 10.1006/taap.2000.8957. [PubMed: 10896851]

Knaapen AM, Shi T, Borm PJ, and Schins RP 2002. Soluble metals as well as the insoluble particle fraction are involved in cellular DNA damage induced by particulate matter. In Oxygen/nitrogen radicals: Cell injury and disease, ed. Vallyathan V, Castranova V, and Shi X, 317–26. Boston, MA: Springer.

Larsson F, Andersson P, Blomqvist P, and Mellander BE 2017. Toxic fluoride gas emissions from lithium-ion battery fires. Scientific Reports 7 (1):1–13. doi: 10.1038/s41598-017-09784-z. [PubMed: 28127051]

Liao Z, Zhang S, Li K, Zhang G, and Habetler TG 2019. A survey of methods for monitoring and detecting thermal runaway of lithium-ion batteries. Journal of Power Sources 436:226879. doi: 10.1016/j.jpowsour.2019.226879.

Loveridge M, Remy G, Kourra N, Genieser R, Barai A, Lain M, Guo Y, Amor-Segan M, Williams M, Amietszajew T, et al. 2018. Looking deeper into the Galaxy (Note 7). Batteries 4 (1):3. doi: 10.3390/batteries4010003.

Mao N, Wang ZR, Chung YH, and Shu CM 2019. Overcharge cycling effect on the thermal behavior, structure, and material of lithium-ion batteries. Applied Thermal Engineering 163:114147. doi: 10.1016/j.applthermaleng.2019.114147.

Masoud EM, and Indris S. 2015. Block-shaped pure and doped $Li_4Ti_5O_{12}$ containing a high content of a Li_2TiO_3 dual phase: An anode with excellent cycle life for high rate performance lithium-ion batteries. RSC Advances 5 (130):108058–66. doi: 10.1039/C5RA22745C.

Massé RC, Liu C. Y. Li, Mai L, and Cao G. 2017. Energy storage through intercalation reactions: Electrodes for rechargeable batteries. National Science Review 4 (1): 26–53. doi: 10.1093/nsr/nww093.

Miller L, and Carriveau RR 2019. Energy demand curve variables – An overview of individual and systemic effects. Sustainable Energy Technologies and Assessments 35:172–9. doi: 10.1016/j.seta.2019.07.006.

Nestler T, Schmid R, Münchgesang W, Bazhenov V, Schilm J, Leisegang T, and Meyer DC 2014. Separators-technology review: Ceramic based separators for secondary batteries. American Institute of Physics Conference Proceedings 1597 (1):155–84.

NIOSH, National Institute for Occupational Safety and Health. 1994. NIOSH pocket guide to chemical hazards. National Institute for Occupational Safety and Health, Centers for Disease Control and Prevention, U.S. Dept. of Health and Human Services, Washington, DC.

Nitta N, Wu F, Lee JT, and Yushin G. 2015. Li-ion battery materials: Present and future. Materials Today 18 (5):252–64. doi: 10.1016/j.mattod.2014.10.040.

NTSB, National Transportation Safety Board. 2014. Auxiliary power unit battery fire Japan airlines Boeing 787–8, JA829J, Boston, Massachusetts, January 7, 2013. NTSB/AIR-14/01, Washington, DC. https://ntsb.gov/investigations/AccidentReports/Reports/AIR1401.pdf.

Paraszczak J, Svedlund E, Fytas K, and Laflamme M. 2014. Electrification of loaders and trucks – a step towards more sustainable underground mining. REPQJ 1 (12):81–6. doi: 10.24084/repqj12.240.

Park YS, and Lee SM 2009. Effects of particle size on the thermal stability of lithiated graphite anode. Electrochimica Acta 54 (12):3339–43. doi: 10.1016/j.electacta.2008.12.030.

Peng Y, Yang L, Ju X, Liao B, Ye K, Li L, Cao B, and Ni Y. 2020. A comprehensive investigation on the thermal and toxic hazards of large format lithium-ion batteries with $LiFePO_4$ cathode. Journal of Hazardous Materials 381:120916. doi: 10.1016/j.jhazmat.2019.120916.

Pfrang A, Kriston A, Ruiz V, Lebedeva N, and di Persio F. 2017. Safety of rechargeable energy storage systems with a focus on Li-ion technology. In Emerging nanotechnologies in rechargeable energy storage systems, ed. Rodriguez-Martinez LM and Omar N, 253–90. Boston, MA: Elsevier.

Raja M, Sanjeev G, Kumar TP, and Stephan AM 2015. Lithium aluminate-based ceramic membranes as separators for lithium-ion batteries. Ceramics International 41 (2):3045–50. doi: 10.1016/j.ceramint.2014.10.142.

Ranjbar N, and Kuenzel C. 2017. Cenospheres: A review. Fuel 207:1–12. doi: 10.1016/j.fuel.2017.06.059.

Ruiz V, and Pfrang A. 2018. JRC exploratory research: Safer Li-ion batteries by preventing thermal propagation-Workshop report: Summary & outcomes. Publications Office of the European Union, Luxembourg.

Samsung. 2017. Galaxy Note7: What we discovered. Accessed December 16, 2020. https://news.samsung.com/global/infographic-galaxy-note7-what-we-discovered.

Sony. 2006. Statement regarding Sony's support of Apple's recall of lithium ion battery packs used in apple notebook computers. Accessed December 16, 2020. https://sony.net/SonyInfo/News/Press/200608/06-0825E/.

Sun J, Li J, Zhou T, Yang K, Wei S, Tang N, Dang N, Li H, Qiu X, and Chen L. 2016. Toxicity, a serious concern of thermal runaway from commercial Li-ion battery. Nano Energy 27:313–9. doi: 10.1016/j.nanoen.2016.06.031.

Valavanidis A, Salika A, and Theodoropoulou A. 2000. Generation of hydroxyl radicals by urban suspended particulate air matter. The role of iron ions. Atmospheric Environment 34 (15):2379–86. doi: 10.1016/S1352-2310(99)00435-5.

Varaschin J, and De Souza E. 2015. Economics of diesel fleet replacement by electric mining equipment. Proceedings of the 15th North American Mine Ventilation Symposium: 328–35. https://vtechworks.lib.vt.edu/handle/10919/89645.

Wang Q, Ping P, Zhao X, Chu G, Sun J, and Chen C. 2012. Thermal runaway caused fire and explosion of lithium ion battery. Journal of Power Sources 208:210–24. doi: 10.1016/j.jpowsour.2012.02.038.

Wierzbicki T, and Sahraei E. 2013. Homogenized mechan- ical properties for the jellyroll of cylindrical Lithium-ion cells. Journal of Power Sources 241:467–76. doi: 10.1016/j.jpowsour.2013.04.135.

Wilson MR, Lightbody JH, Donaldson K, Sales J, and Stone V. 2002. Interactions between ultrafine particles and transition metals in vivo and in vitro. Toxicology and Applied Pharmacology 184 (3):172–9. doi: 10.1006/taap.2002.9501. [PubMed: 12460745]

Yang Y, Wang Z, Guo P, Chen S, Bian H, Tong X, and Ni L. 2021. Carbon oxides emissions from lithium-ion batteries under thermal runaway from measurements and predictive model. Journal of Energy Storage 33:101863. doi: 10.1016/j.est.2020.101863.

Yim CH, Courtel FM, and Abu-Lebdeh Y. 2013. A high capacity silicon–graphite composite as anode for lithium-ion batteries using low content amorphous silicon and compatible binders. Journal of Materials Chemistry A 1 (28):8234–43. doi: 10.1039/c3ta10883j.

Yuan L, Dubaniewicz T, Zlochower I, Thomas R, and Rayyan N. 2020. Experimental study on thermal runaway and vented gases of lithium-ion cells. Process Safety and Environmental Protection 144:186–92. doi: 10.1016/j.psep.2020.07.028.

Zhao W, Luo G, and Wang CY 2015. Modeling internal shorting process in large-format Li-ion cells. Journal of the Electrochemical Society 162 (7):A1352–A1364. doi: 10.1149/2.1031507jes.

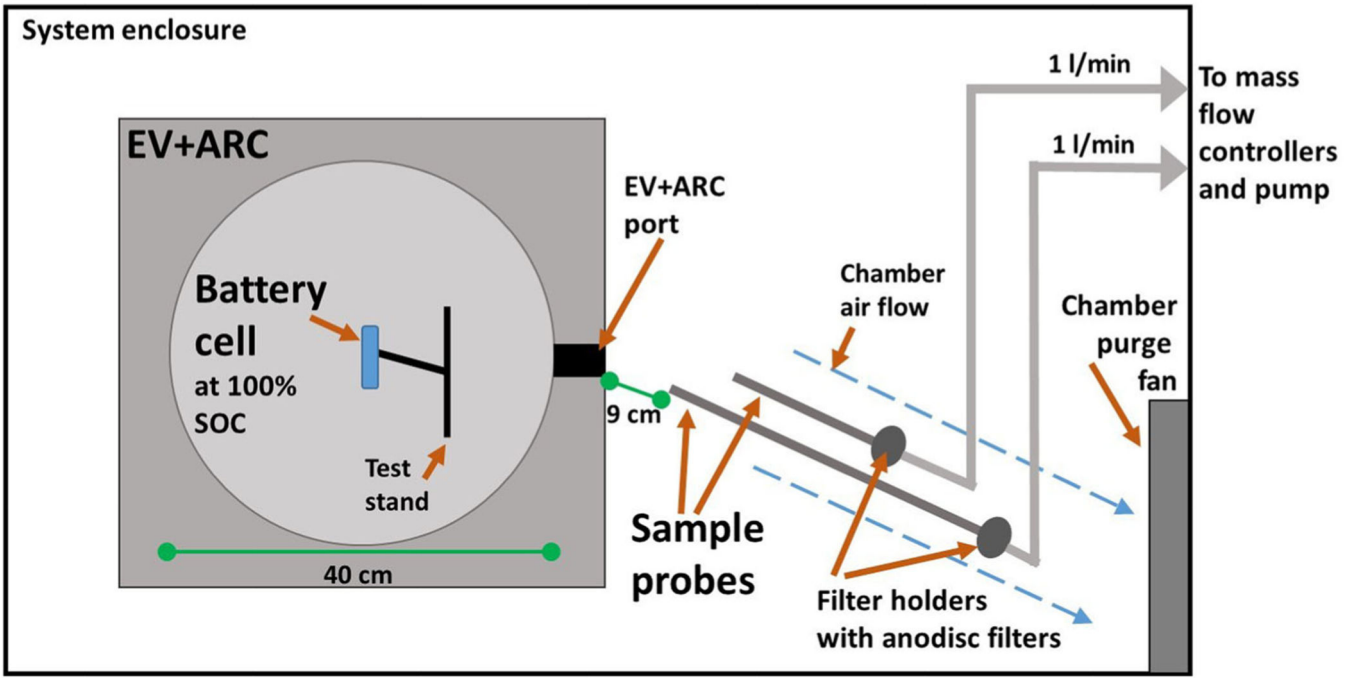

Figure 1.
Experimental setup for the collection of lithium-ion battery explosion aerosols on filter media.

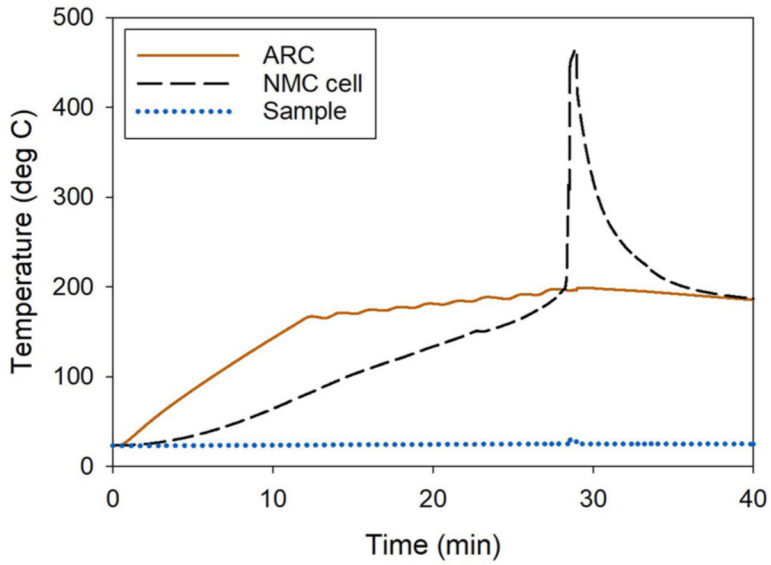

Figure 2.
Temperature of the ARC, NMC cell, and filter sample inlet during the thermal runaway test.

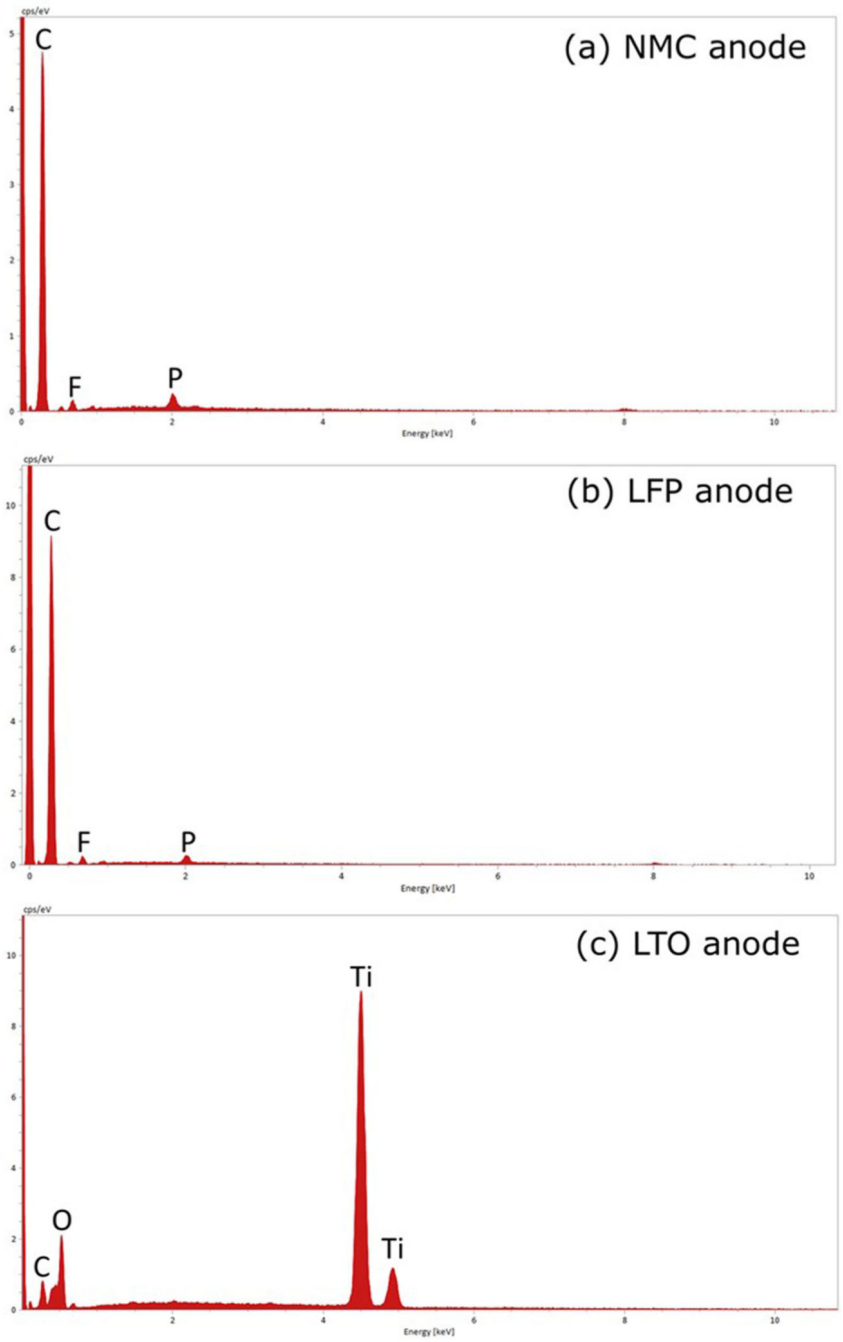

Figure 3.
EDS spectra of the (a) NMC, (b) LFP, and (c) LTO battery anodes.

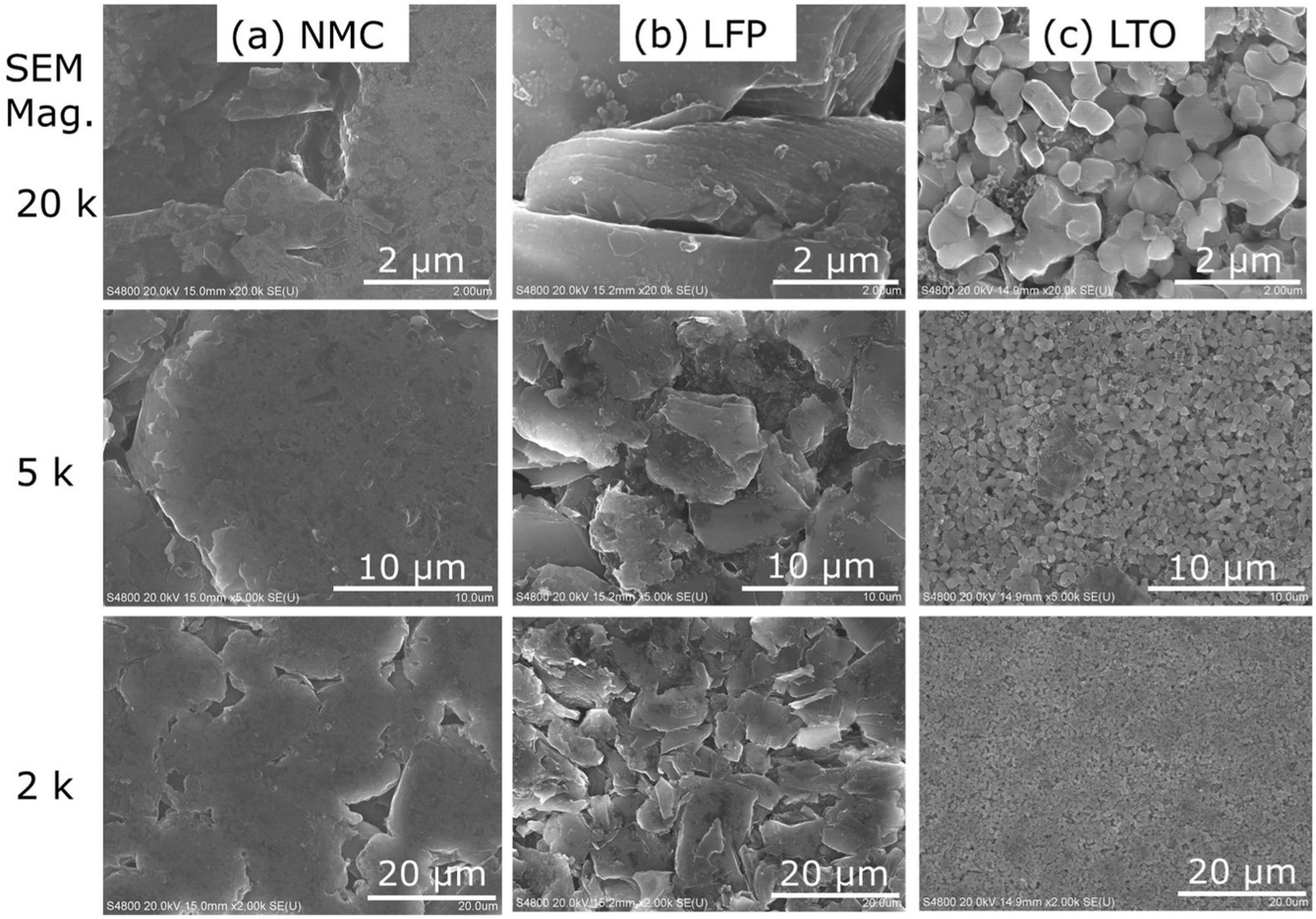

Figure 4.
SEM images at 2, 5, and 20 k magnification of the anode for the (a) NMC, (b) LFP, and (c) LTO battery cells.

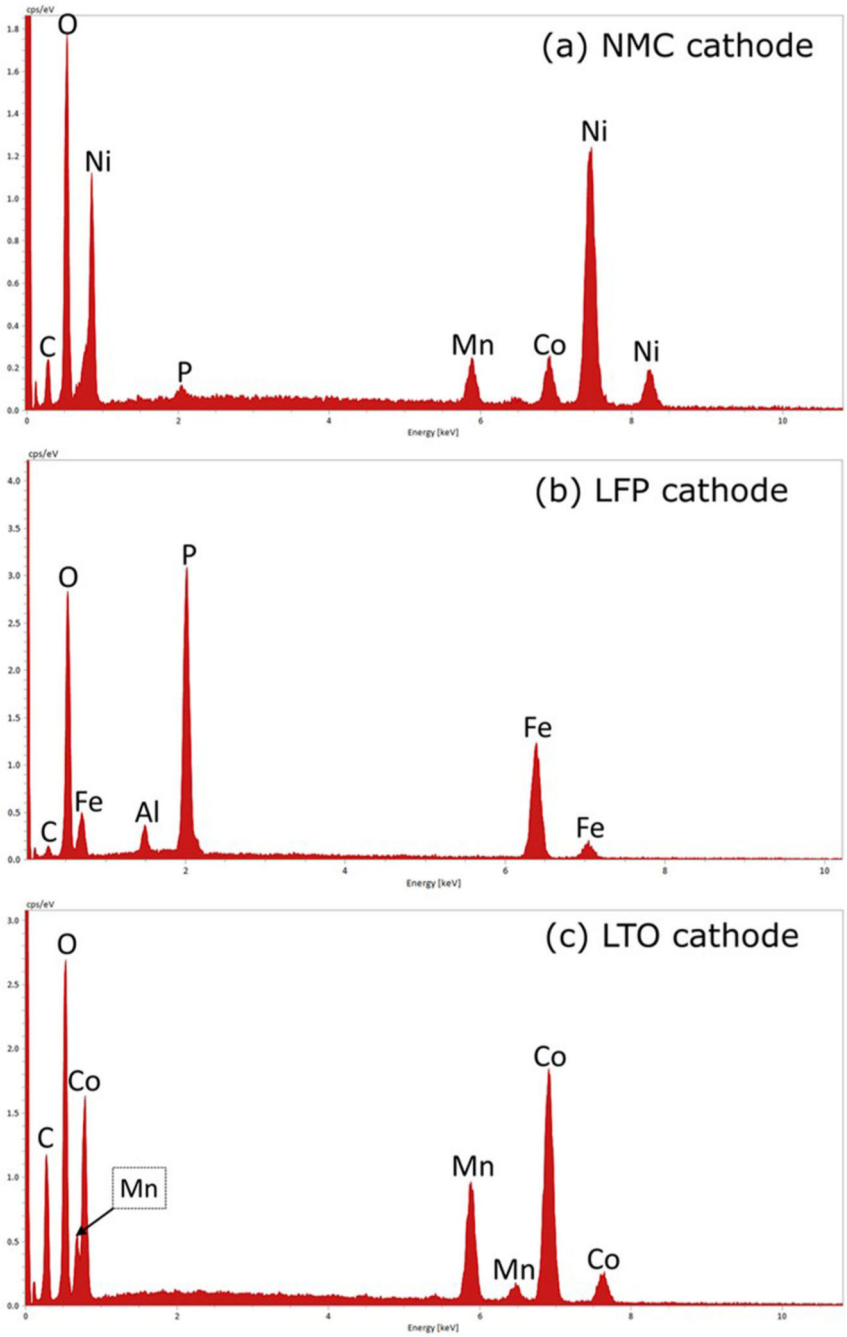

Figure 5.
EDS spectra of the (a) NMC, (b) LFP, and (c) LTO battery cathodes.

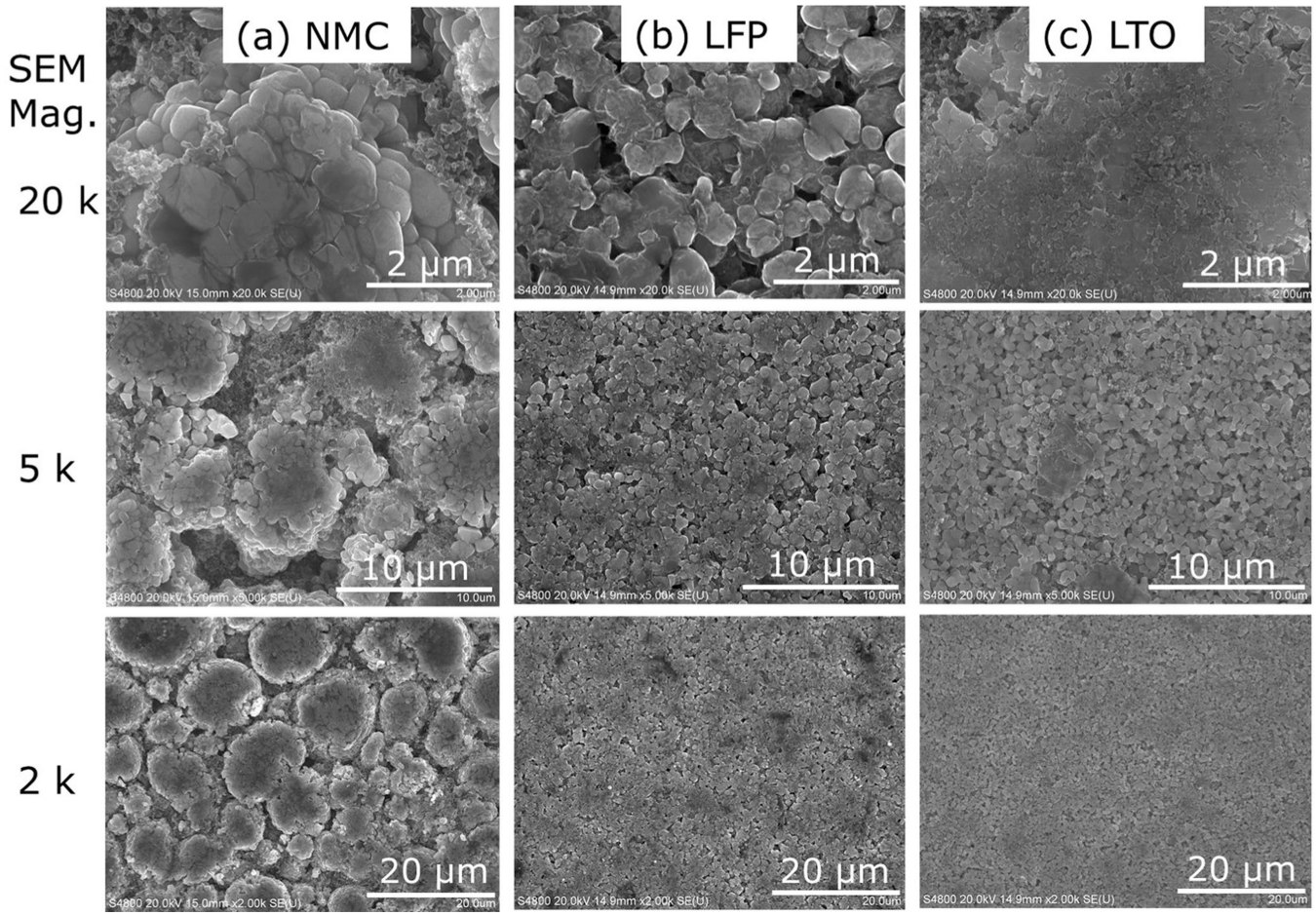

Figure 6.
SEM images 2, 5, and 20 k magnification of the cathode for the (a) NMC, (b) LFP, and (c) LTO battery cells.

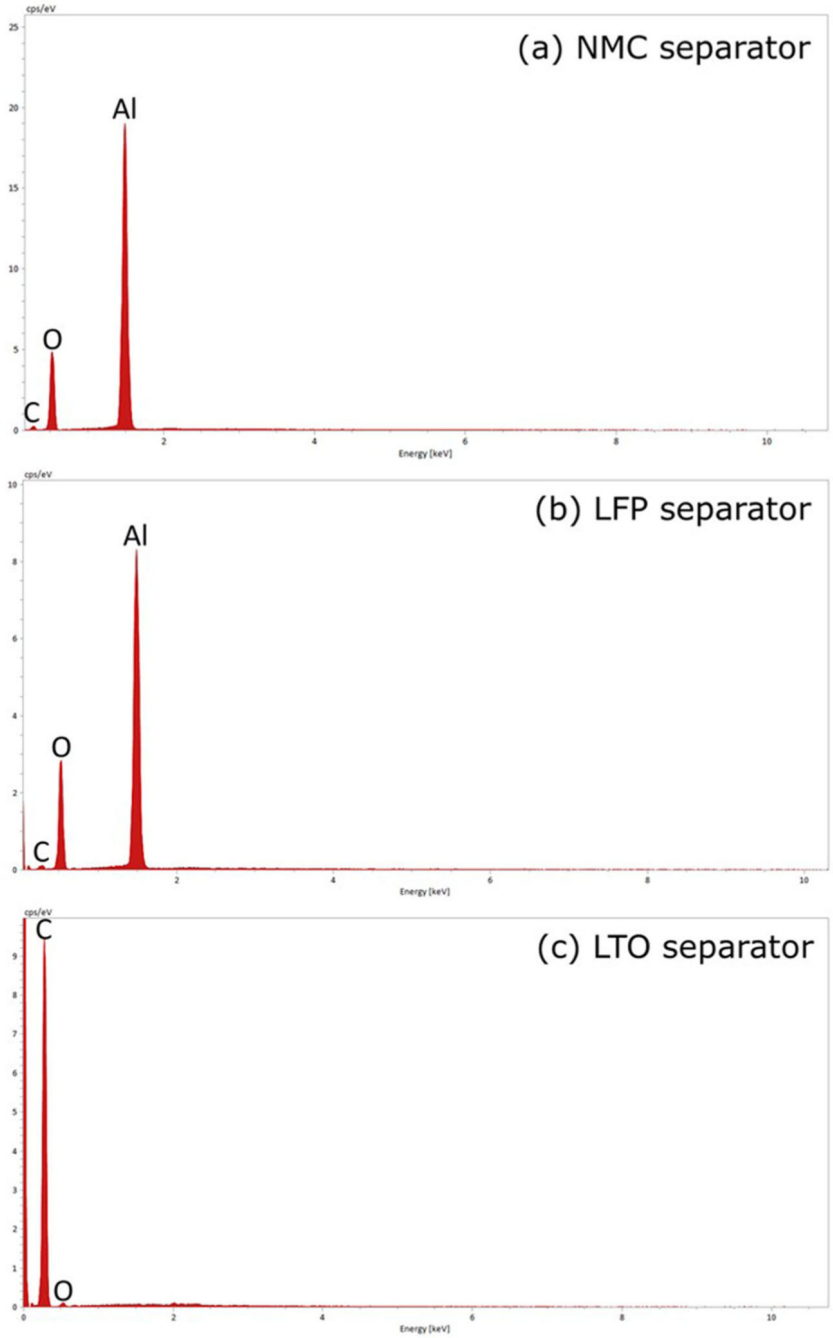

Figure 7.
EDS spectra of the (a) NMC, (b) LFP, and (c) LTO battery separators.

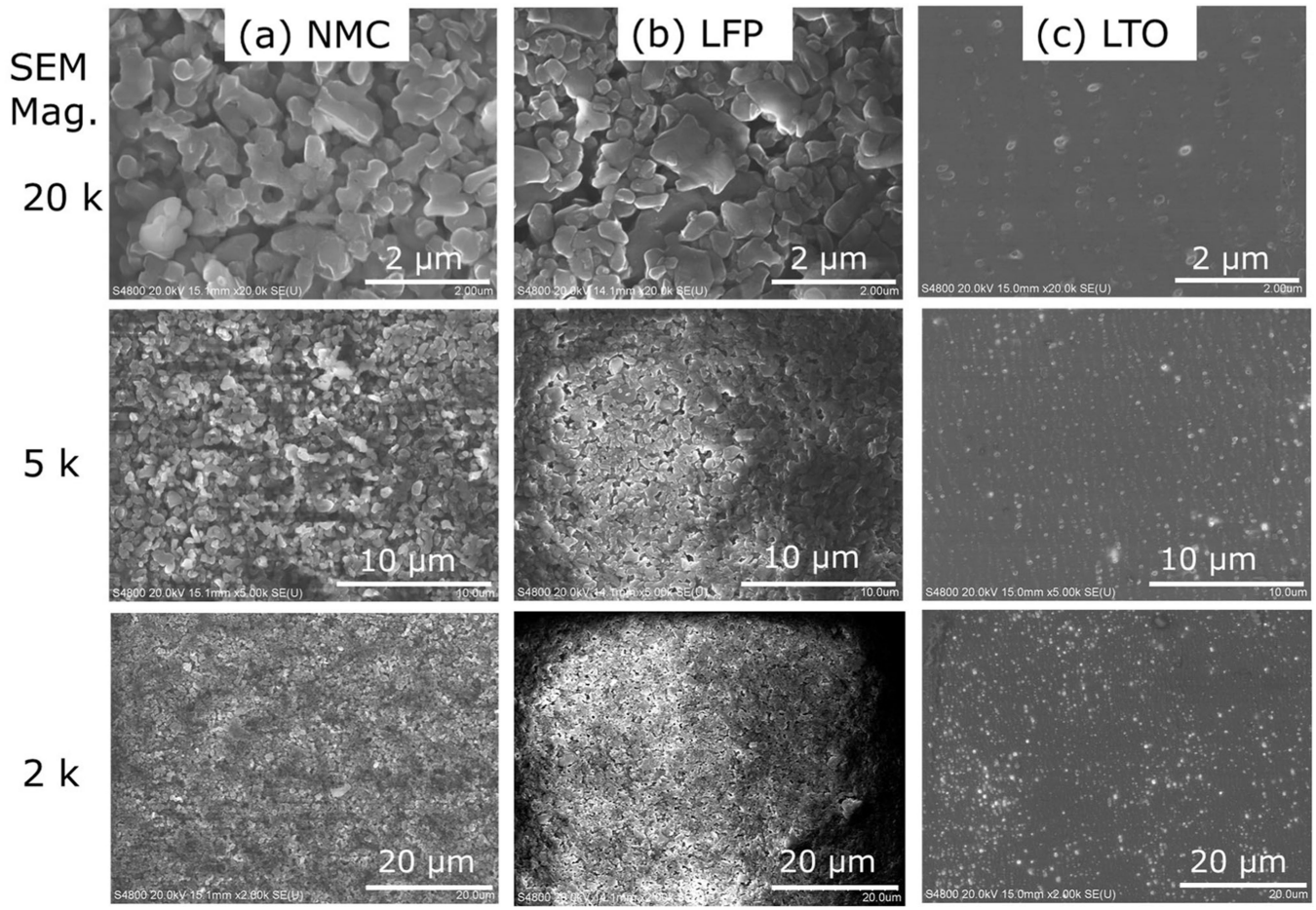

Figure 8.

SEM images 2, 5 and 20 k magnification of the separator for the (a) NMC, (b) LFP and (c) LTO battery cells.

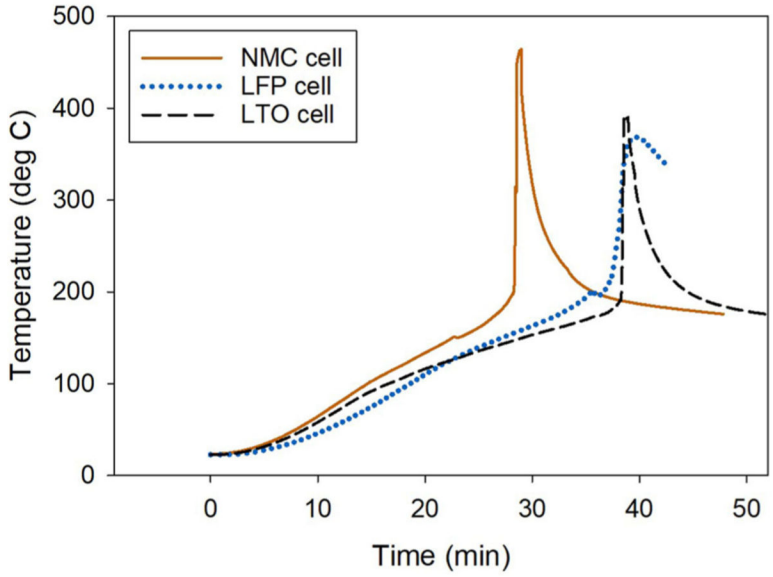

Figure 9.
Battery temperature during ARC tests for the NMC, LFP, and LTO cells.

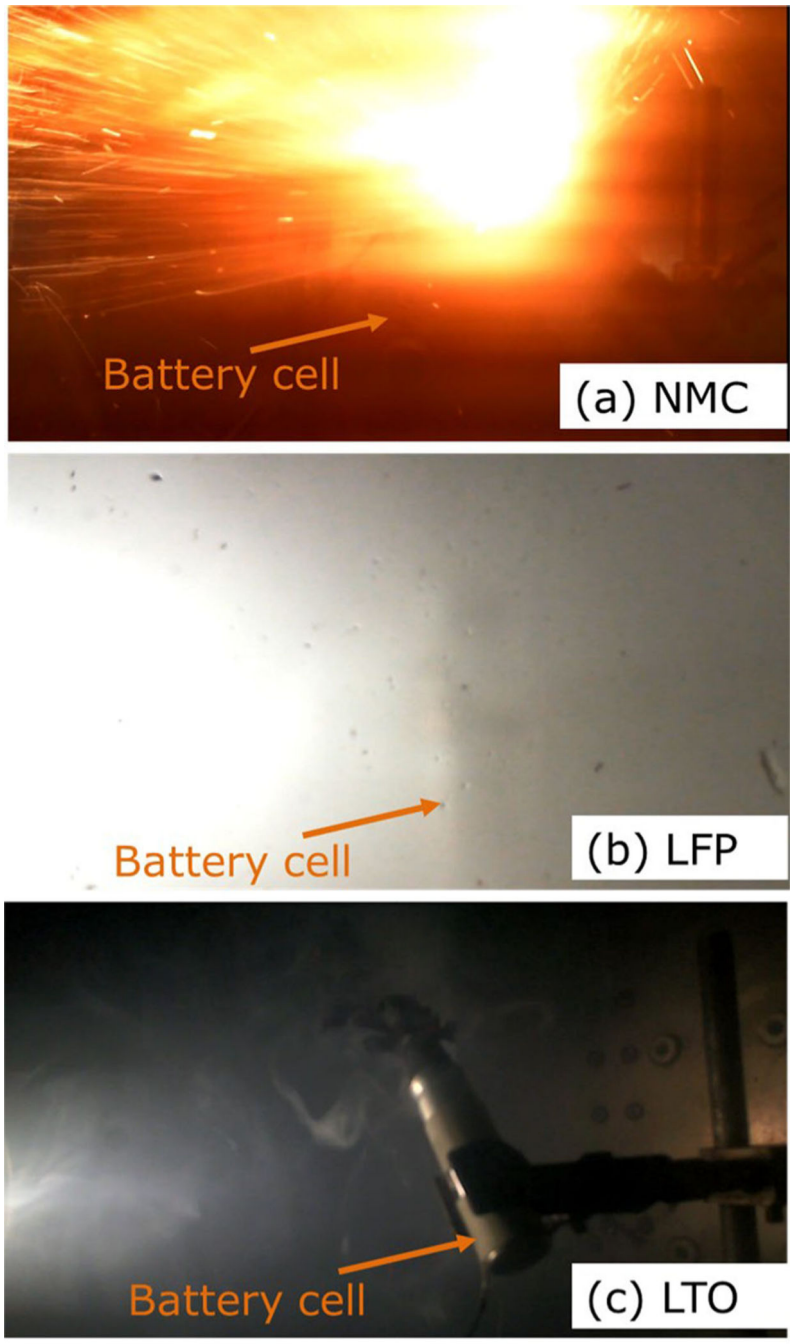

Figure 10.
Snapshots of the ARC test videos showing the intense part of thermal runaway for the (a) NMC, (b) LFP, and (c) LTO cells.

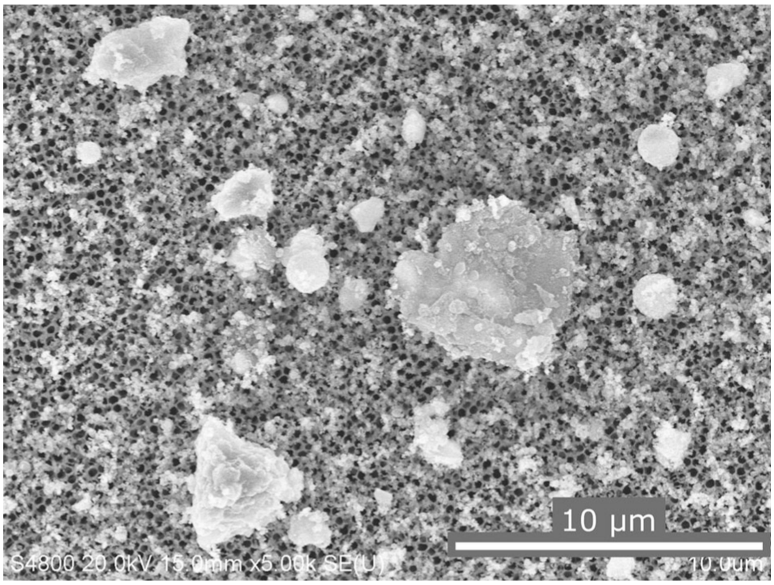

Figure 11.
SEM image of NMC cell explosion aerosols collected on an anodisc membrane with a 5-sec sampling time. The black pores of the anodisc membrane are visible below the collected aerosols.

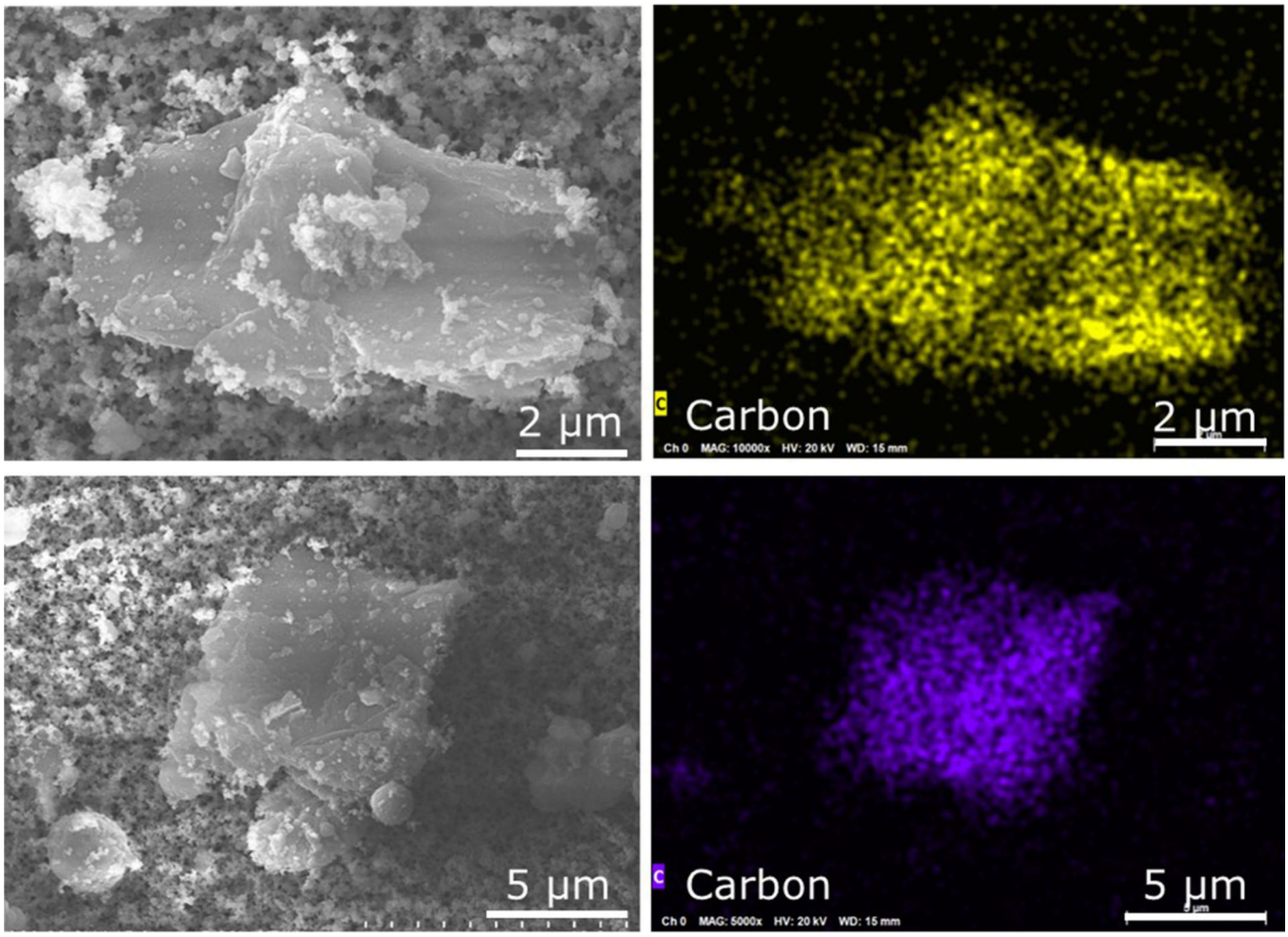

Figure 12.
EDS mapping of carbonaceous faceted particles indicative of anode material in NMC explosion aerosols.

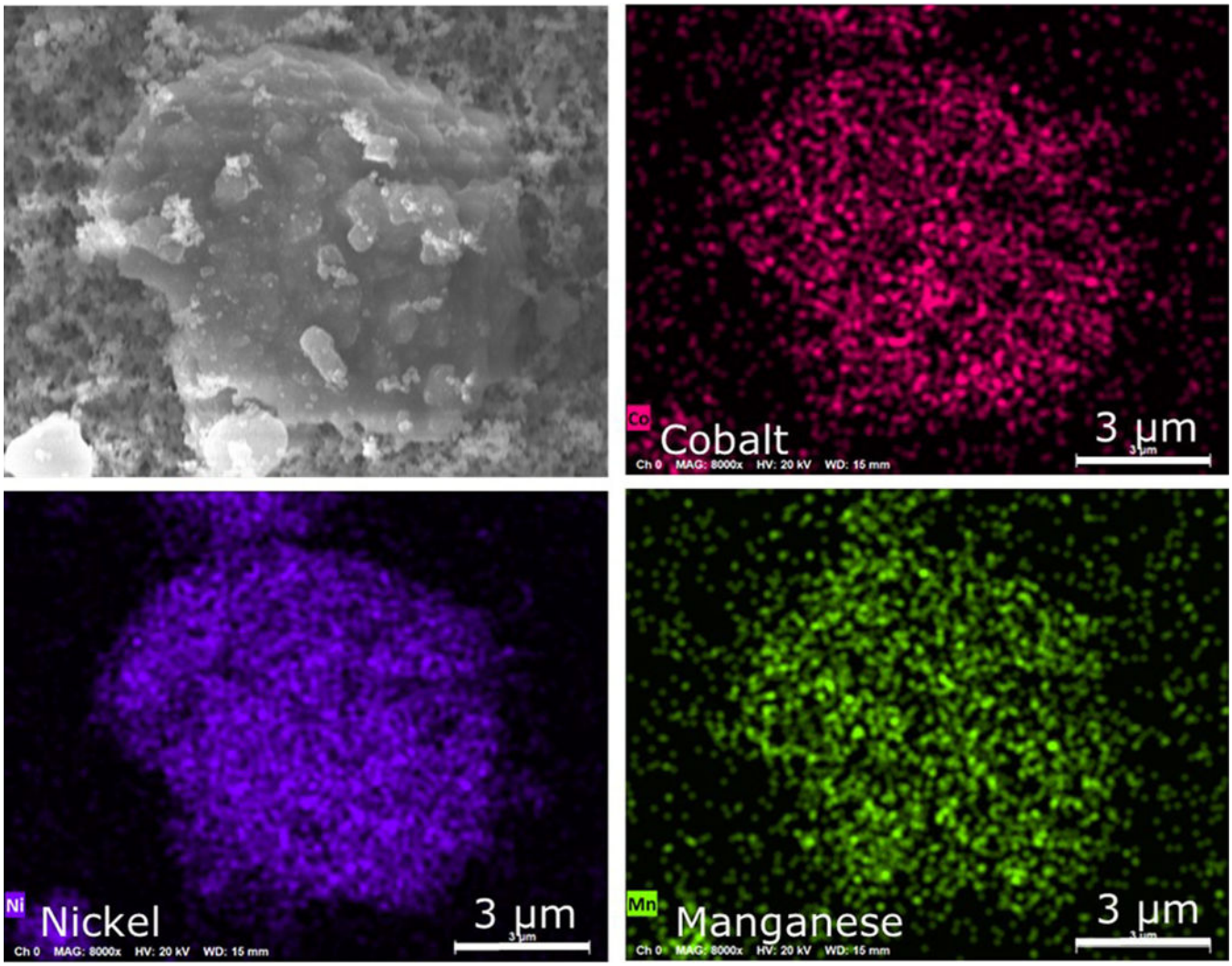

Figure 13.
EDS mapping of particle in NMC explosion aerosols that contained cathode materials of nickel, manganese, and cobalt.

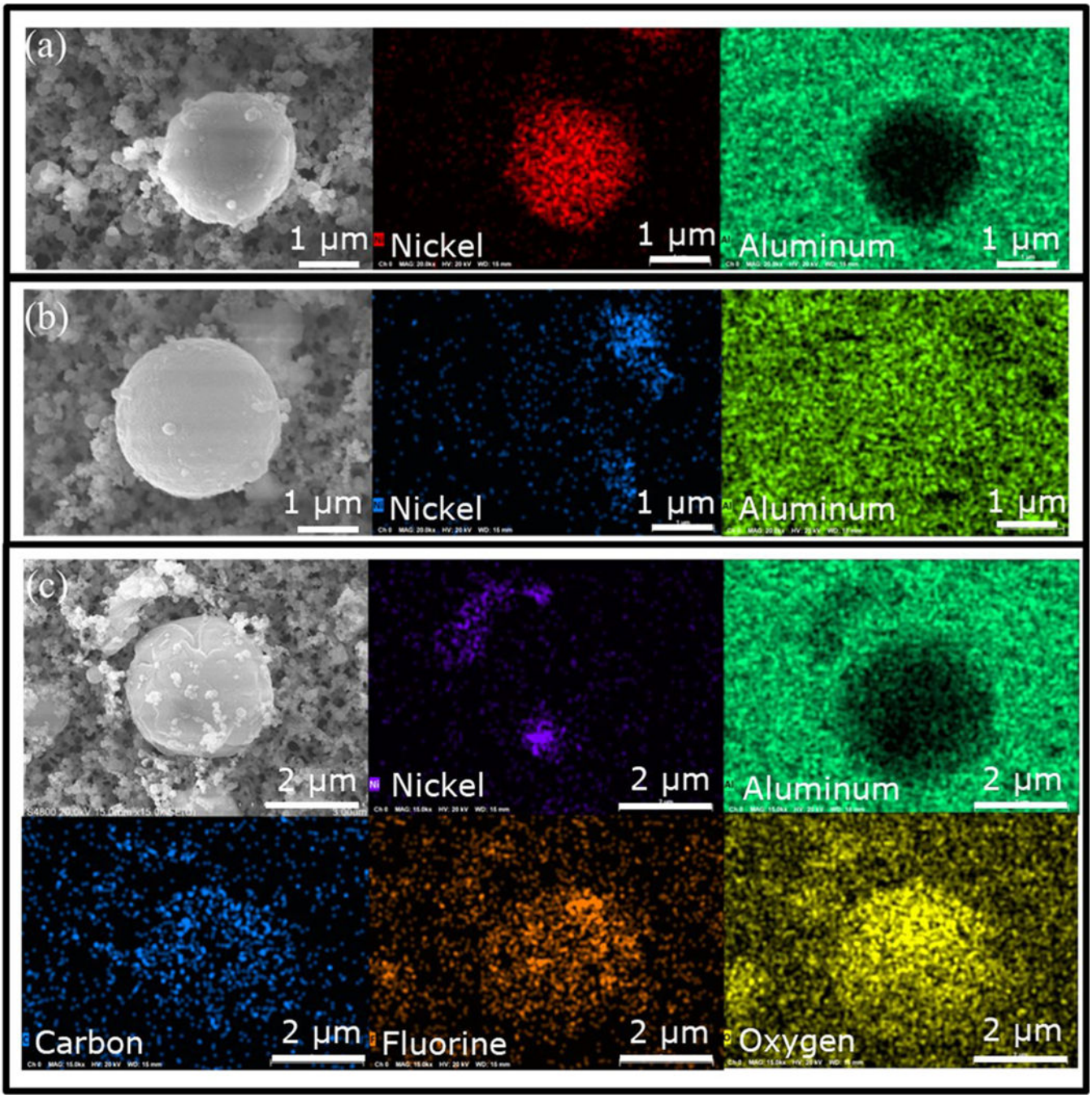

Figure 14.
EDS mapping of microspheres in NMC explosion aerosols. (a) Nickel microsphere (red) on aluminum substrate (green). (b) Aluminum microsphere (green) near smaller nickel particles (blue) on aluminum substrate (green). (c) Microsphere containing carbon (blue), fluorine (orange), and oxygen (yellow) with adjacent nickel particles (indigo) on aluminum substrate (green).

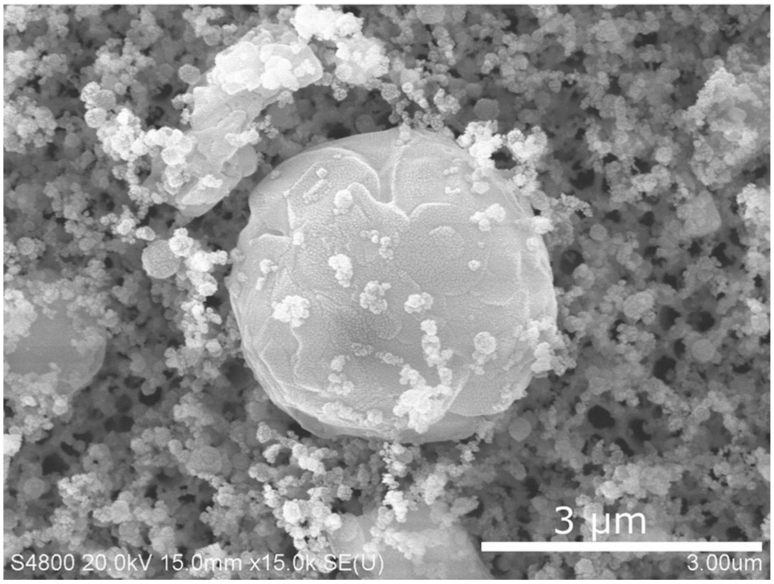

Figure 15.
SEM image of nanoparticles and microsphere in NMC explosion aerosols.

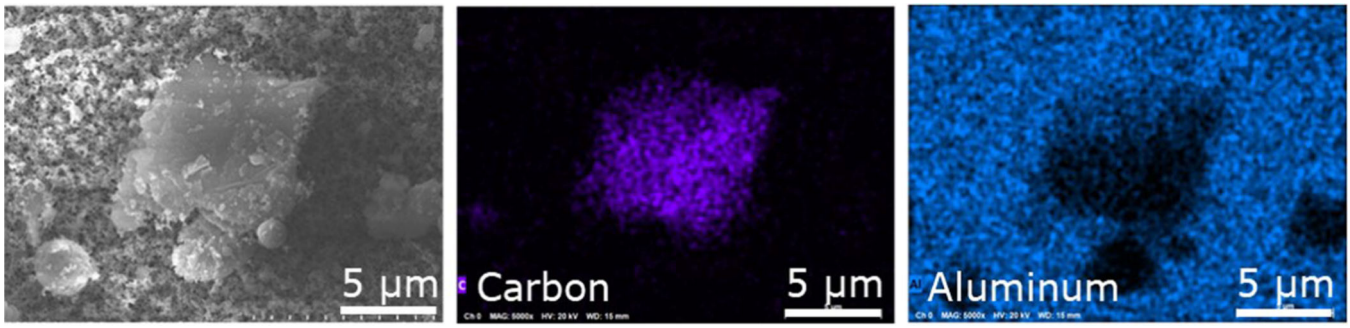

Figure 16.
Nanoparticles around large carbonaceous particle appear to be composed of aluminum (teal) rather than carbon (indigo).

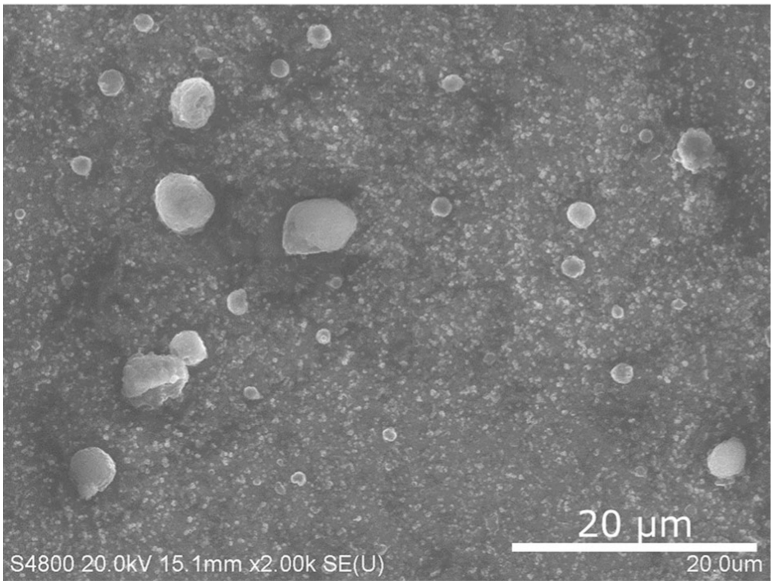

Figure 17.
SEM image of LFP explosion aerosols on anodisc filter.

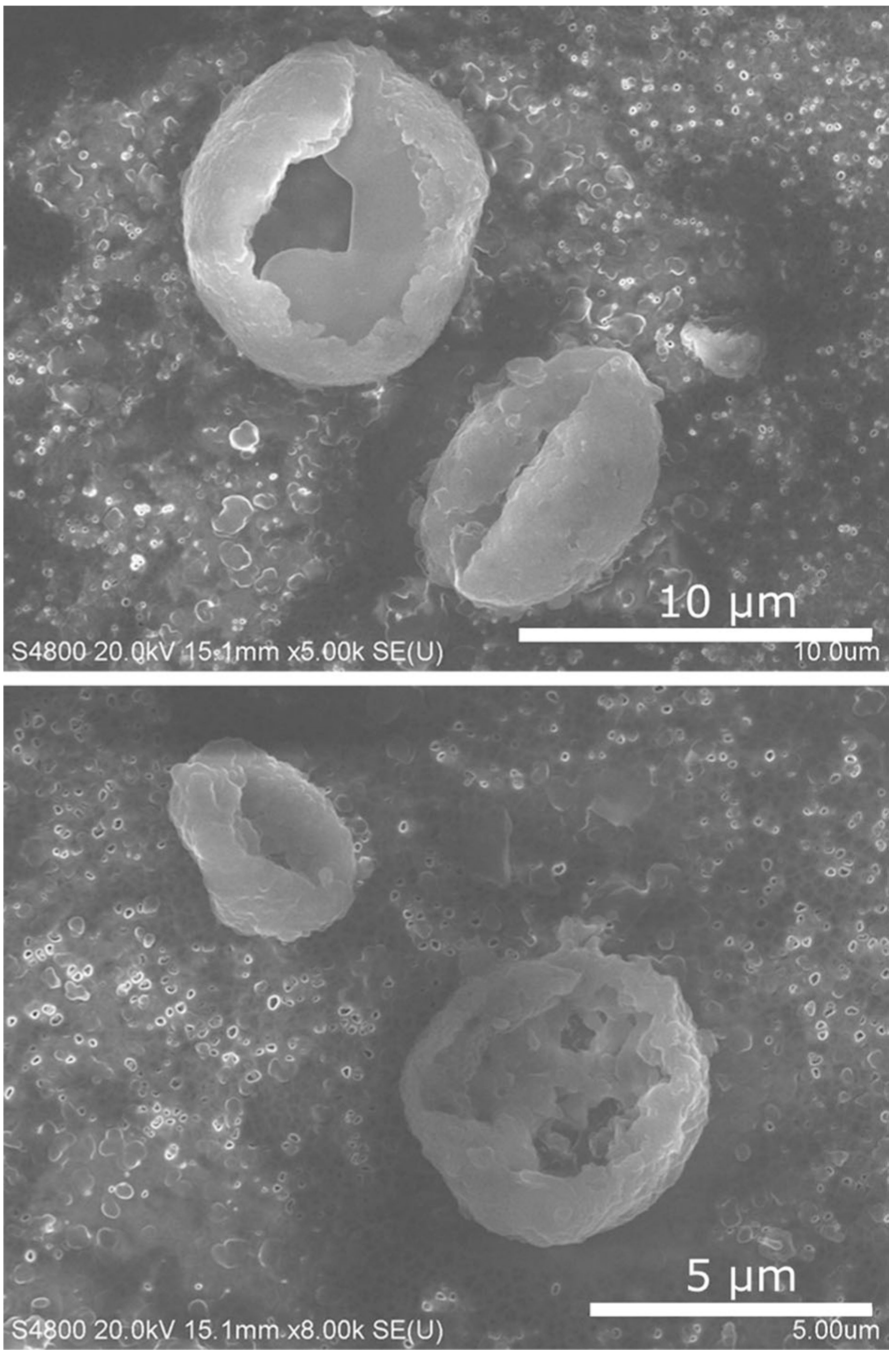

Figure 18.
SEM images of carbonaceous cenospheres emitted by LFP explosion.

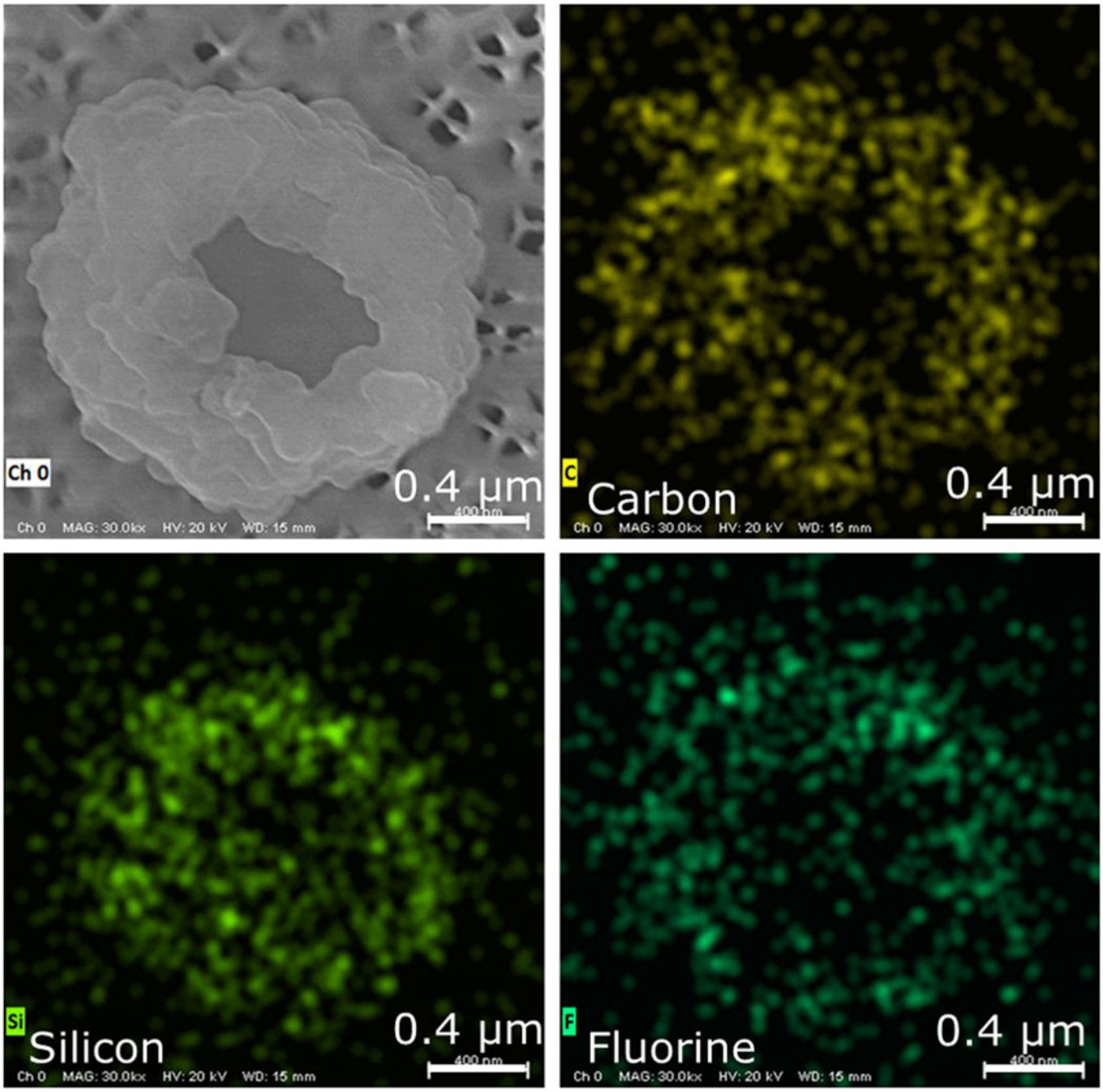

Figure 19.
EDS mapping of cenosphere in LPF explosion aerosols that contains carbon, fluorine, and silicon.

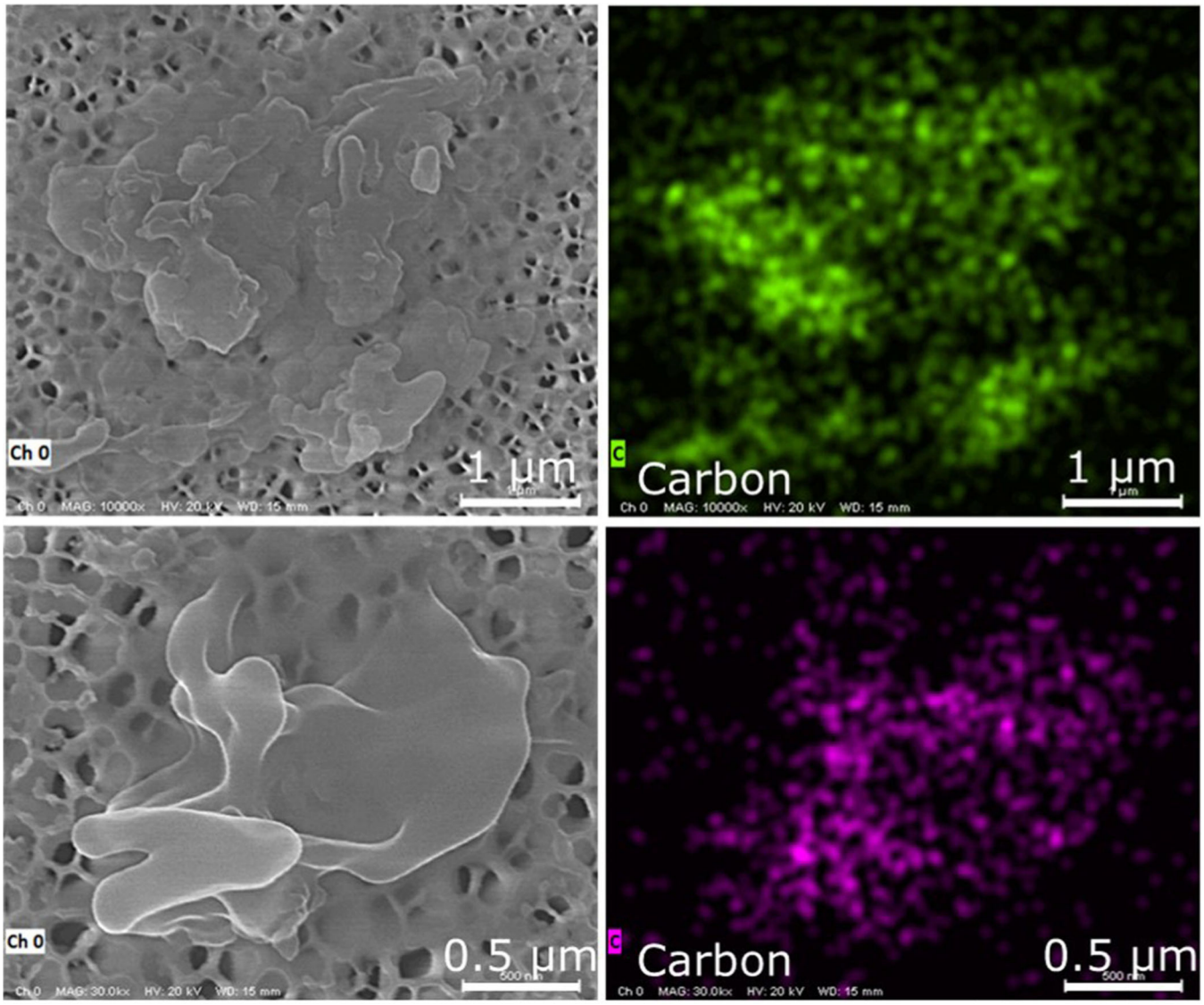

Figure 20.
EDS mapping of carbon material in LFP explosion aerosols.

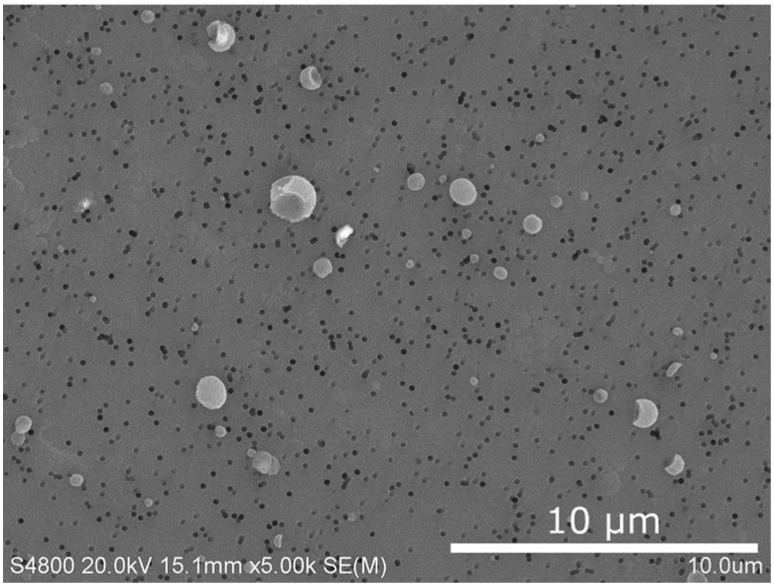

Figure 21.
SEM images of LTO explosion aerosols on a nuclepore membrane filter.

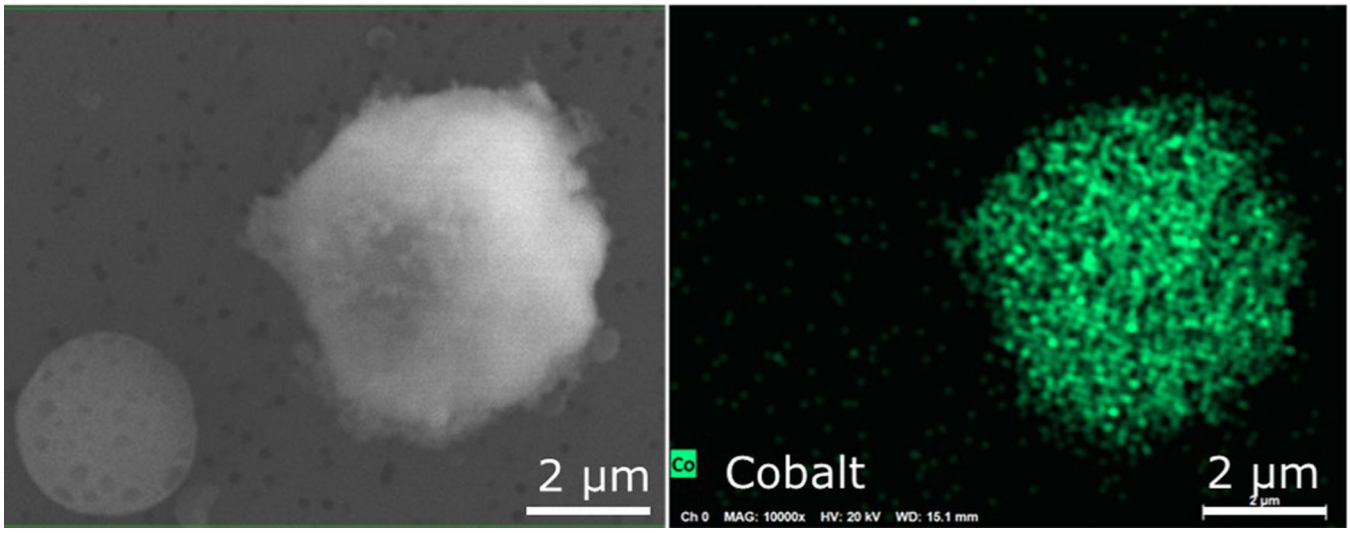

Figure 22.

EDS mapping of LTO explosion particle containing cobalt. The results for the porous particle on the left were not clear probably due to its low effective density.